Solid-State Electrochemical Protonation of $SrCoO_{2.5}$ into $H_xSrCoO_{2.5}$ (x = 1, 1.5 and 2)

Qian Yang[a*], Joonhyuk Lee[b], Hyoungjeen Jeen[b], Hai Jun Cho[c], and Hiromichi Ohta[c*]

[a] *Graduate School of Information Science and Technology, Hokkaido University, N14W9, Kita, Sapporo 060-0814, Japan*

[b] *Department of Physics, Pusan National University, Busan 46241, South Korea*

[c] *Research Institute for Electronic Science, Hokkaido University, N20W10, Kita, Sapporo 001-0020, Japan*

*Email: yangqian@eis.hokudai.ac.jp, hiromichi.ohta@es.hokudai.ac.jp

KEYWORDS: solid-state electrochemical protonation, brownmillerite, $H_xSrCoO_{2.5}$, $SrCoO_{2.5}$, optical property, magnetic property

ABSTRACT: Among many transition metal oxides (TMOs), strontium cobalt oxide ($SrCoO_x$) is a promising active material for advanced memory devices due to the

versatile valence state of cobalt ion. Several $SrCoO_x$-based electrochemical devices have been proposed, but solid-state protonation from $SrCoO_{2.5}$ to $H_xSrCoO_{2.5}$ (x = 1, 1.5, and 2) at room temperature has not been demonstrated thus far due to the absence of appropriate solid electrolyte. Here we demonstrate a solid-state electrochemical protonation of $SrCoO_{2.5}$ using mesoporous amorphous $12CaO \cdot 7Al_2O_3$ (CAN) film as the solid electrolyte. The crystalline phase discretely changed from $SrCoO_{2.5}$ to $HSrCoO_{2.5}$ (phase A), $H_{1.5}SrCoO_{2.5}$ (phase B), and $H_2SrCoO_{2.5}$ (phase C) through formation of an intermediate phase of $H_{1.25}SrCoO_{2.5}$. The $H_{1.5}SrCoO_{2.5}$ (phase B) was colorless-transparent and showed weak ferromagnetism. The present results indicate that the CAN film can be used as the solid electrolyte for the protonation treatment of TMOs.

INTRODUCTION

Due to the recent explosive increase in the stored volume of information, advanced memory devices that store multiple information are highly demanded[1]. Materials that show non-volatile control of the optical, electrical, and magnetic properties would be useful as the active material of these advanced memory devices. In this regard, transition metal oxides (TMOs) are promising active materials of such memory devices

since many TMOs show the transition from one crystalline phase to another by electrochemical protonation/reduction/oxidation method, resulting in the changes in optoelectronic and magnetic properties[2-6].

Among many TMOs, we focused on $SrCoO_x$ film in this study because $SrCoO_x$ film is known as an oxygen sponge[7]; where the topotactic redox reaction of $SrCoO_x$ easily occurs[8]. There are several crystalline phases associated with the valence state of Co ions: brownmillerite (BM) $SrCoO_{2.5}$ (Co^{3+}), perovskite $SrCoO_3$ (Co^{4+}), and protonated BM-$H_xSrCoO_{2.5}$ (Co^{2+}) (x = 1, 1.5, and 2)[5, 9]. BM-$SrCoO_{2.5}$ is a brown-colored antiferromagnetic insulator, and $SrCoO_3$ is a black-colored ferromagnetic metal. Further, protonated $H_xSrCoO_{2.5}$, which is almost transparent in the visible region, is an electrical insulator and shows a weak ferromagnetic behavior[5]. In addition, the thermal conductivity of $SrCoO_x$ also can be modulated by the electrochemical protonation/oxidation treatment[10]. Thus, we can control the optical, electrical, magnetic, and thermal properties of $SrCoO_x$, which can be utilized in the active material for the electrochemical memory device.

In 2017, Lu *et al*.[5] firstly demonstrated the electrochemical protonation/oxidation of

$SrCoO_x$ and successfully controlled the optical, electrical, and magnetic properties. They used residual water in the ionic liquid as the electrolyte. Since there is a possibility of liquid leakage from the device, utilization of liquid electrolyte[5, 11] is not appropriate for the requirement for the practical application. To overcome this problem, the use of the solid electrolyte is essential for realizing a leakage-free device. In 2016, Katase *et al*.[12] used a porous amorphous $NaTaO_3$ film as the solid electrolyte and successfully converted $SrCoO_{2.5}$ film to $SrCoO_3$ film at room temperature. In our preliminary experiment, we tried the protonation of $SrCoO_{2.5}$ film using $NaTaO_3$ film as the solid electrolyte but failed, probably due to the strong alkalinity of $NaTaO_3$ containing NaOH[12-13].

In this study, we focused on the solid-state electrochemical protonation of $SrCoO_{2.5}$ into $H_2SrCoO_{2.5}$. We choose a mesoporous amorphous $12CaO \cdot 7Al_2O_3$ (CAN)[14-15] film as the solid electrolyte. CAN contain ultrapure water in the mesopores (~40 vol.%) and shows the electrical conductivity of 2.2×10^{-9} S cm^{-1}, which is ~4% of that of ultrapure water (5.5×10^{-8} S cm^{-1}) at room temperature[16]. Katase *et al*. demonstrated that VO_2[17-18] and WO_3[19] can be protonated electrochemically using CAN as the solid electrolyte at room temperature. Thus, we expected that solid-state electrochemical protonation of $SrCoO_{2.5}$

is possible by using CAN as the solid electrolyte. As a result of this study, we successfully modulated the crystalline phase discretely from $SrCoO_{2.5}$ to $HSrCoO_{2.5}$ (phase A), $H_{1.5}SrCoO_{2.5}$ (phase B), and $H_2SrCoO_{2.5}$ (phase C) through the formation of an intermediate phase of $H_{1.25}SrCoO_{2.5}$. $H_{1.5}SrCoO_{2.5}$ (phase B) was colorless-transparent and showed weak ferromagnetism. The present results indicate that the CAN film can be used as the solid electrolyte for the protonation treatment of TMOs.

EXPERIMENTAL SECTION

Sample preparation: Two-terminal electrochemical cells were fabricated by a pulsed laser deposition (PLD) technique with stencil masks (**Fig. 1a**). First, ~30-nm-thick 10 mol% Nb-doped $SrTiO_3$ films were heteroepitaxially grown on (001)-oriented $SrTiO_3$ substrate (10 mm × 10 mm × 0.5 mm) at the substrate temperature of 900 °C in an oxygen atmosphere (1×10^{-3} Pa). Second, ~50-nm-thick $SrCoO_{2.5}$ active layers were heteroepitaxially grown on the Nb-doped $SrTiO_3$ films with stencil mask (2.25 mm × 2.25 mm) at the substrate temperature of 850 °C in an oxygen atmosphere (10 Pa). Then, ~300-nm-thick mesoporous CAN containing ~40 vol.% water was deposited on the $SrCoO_{2.5}$ film at room temperature as the solid electrolyte. Finally, ~30-nm-thick

ITO film was deposited as the top electrode at room temperature. Details of the PLD condition of each layer have been published elsewhere[12, 14-15, 17, 19-22].

Electrochemical oxidation and protonation: Electrochemical protonation of $SrCoO_{2.5}$ films was performed at room temperature in air as schematically shown in **Fig. 1**. When a constant voltage of +10 V was applied using a source meter (Model 2450, Keithley), the $SrCoO_{2.5}$ film was converted into $H_xSrCoO_{2.5}$ film within several hours.

Crystallographic analyses: The crystallographic phase and orientation were analyzed using a high-resolution X-ray diffractometer with Cu $K\alpha_1$ (λ = 1.54059 Å) radiation (ATX-G, Rigaku Co.). Out-of-plane Bragg diffraction pattern and reciprocal space mapping of the samples were measured at room temperature. *In-situ* monitoring of the out-of-plane XRD patterns during the electrochemical reduction was performed using a high-resolution X-ray diffractometer with Cu $K\alpha_1$ (λ = 1.54059 Å) radiation (D8 Advance, Bruker) and a source meter (Model 2450, Keithley). After applying the bias voltage using gold-coated probes, all the *in-situ* XRD patterns were measured at room temperature in air. Each scan took about 5 minutes and was plotted in a two-dimensional contour diagram.

Magnetic properties: The magnetic moments of the protonated/as-grown/oxidized samples were measured at 10−300 K with 100 Oe field cooling using a SQUID magnetometer (MPMS3, Quantum Design). To check the change in magnetic properties, magnetic hysteresis loops (*M* vs. *H* curves) were measured up to 7 T at 10 K.

Optical property measurements: The optical transmission spectra of the two-terminal memory devices were measured at room temperature using UV-Vis-NIR spectrometer (SolidSpec-3700, Shimadzu) and FT-IR (Model IRPrestige-21, Shimadzu).

Proton concentration: We conducted secondary-ion mass spectrometry (SIMS) to obtain the hydrogen concentration in the protonated sample (Front Side SIMS, PHI, 6800). Cs^+ primary ion beam (2 keV) was scanned, and data were collected in an area of 40 × 40 μm. The Hydrogen concentration of H^+ ions was quantitatively analyzed by profiling proton-embedded silica with known H^+ doses.

RESULTS AND DISCUSSION

During the protonation, we *in-situ* monitored the out-of-plane XRD pattern of the device as shown in **Fig. 2a**. We also recorded the flowing current density (*J*) to the solid-state electrochemical cell during the voltage application (**Fig. 2b**). Before the protonation (0 min), 008 diffraction peak of BM-$SrCoO_{2.5}$ (008_{BM}) is seen together with 002 $SrTiO_3$ substrate (002s). Approximately 40 min after starting the protonation treatment, 008 diffraction peak of $HSrCoO_{2.5}$ (008_A) appears and the intensity of 008_{BM} becomes weak. The *J* dropped from ~5 mA cm^{-2} to ~4 mA cm^{-2} simultaneously. Approximately 100 min after starting the protonation treatment, 008 diffraction peak of $H_{1.5}SrCoO_{2.5}$ (008_B) appears together with a diffraction peak of the intermediate phase. Details of the intermediate phase are described later. Approximately 260 min after starting the protonation treatment, 008 diffraction peak of $H_2SrCoO_{2.5}$ (008_C) appears. Simultaneously, diffraction peaks of 008_A and intermediate phase disappear. The *J* gradually decreased from ~3.6 mA cm^{-2} to ~0.3 mA cm^{-2}. These results indicate that solid-state protonation is possible by using CAN as the solid electrolyte.

In order to clarify the diffraction peak of the intermediate phase, we measured out-of-plane XRD patterns of the solid-state electrochemical cell (another cell) after protonation treatment (**Fig. 2c**). At 0 min, 00*l* diffraction peaks of BM-$SrCoO_{2.5}$ are

seen together with 00*l* $SrTiO_3$ substrate, indicating strong *c*-axis orientation of the BM-$SrCoO_{2.5}$ film. After starting the protonation treatment, the diffraction peak position changes discretely from $q_z/2\pi = (0.6346 \times l)$ nm^{-1} (BM-$SrCoO_{2.5}$) to $(0.6091 \times l)$ nm^{-1} ($HSrCoO_{2.5}$, A), $(0.5968 \times l)$ nm^{-1} ($H_{1.5}SrCoO_{2.5}$, B), and $(0.5845 \times l)$ nm^{-1} ($H_2SrCoO_{2.5}$, C) through formation of an intermediate phase of $H_{1.25}SrCoO_{2.5}$ ($q_z/2\pi$ = 1.822, 3.046, 4.253, 5.484, and 6.699 nm^{-1}). **Figure 2d** summarizes schematic modification of the crystal structure upon protonation treatment. The lattice parameter *c* of BM-$SrCoO_{2.5}$ is 1.5751 nm, which agrees well with the reported value (1.5745 nm)[23]. The lattice parameter *c* of phase B is 1.6756 nm, which agrees well with that of $H_{1.5}SrCoO_{2.5}$ (1.675 nm)[9]. The intermediate phase $H_{1.25}SrCoO_{2.5}$ is a half-filled state of the oxygen vacancy site of $HSrCoO_{2.5}$ (phase A) with an H_2 dimer. Thus, the lattice parameter *c* is double of phases A and B.

In order to further clarify the formation of $H_{1.5}SrCoO_{2.5}$ (phase B) after 240 min protonation treatment, we measured the hydrogen concentration by SIMS (**Figure S1**). The hydrogen concentration of the $H_{1.5}SrCoO_{2.5}$ (phase B) sample is ~2×10^{22} cm^{-3}. For comparison, we also prepared oxidized $SrCoO_3$ samples by applying negative voltage (−10 V) to the solid-state electrochemical cell for 1 h in air. Compared to the as-

grown $SrCoO_{2.5}$ sample and oxidized $SrCoO_3$ samples, the $H_{1.5}SrCoO_{2.5}$ (phase B) sample is an order of magnitude higher in the hydrogen concentration. The quantitative hydrogen concentration was estimated to be 1.5 H per chemical formula of $SrCoO_{2.5}$, which is close to the reported phase $H_{1.5}SrCoO_{2.5}$[9].

Then, we measured the optical transmission spectra of the as-grown BM-$SrCoO_{2.5}$ sample, the protonated $H_{1.5}SrCoO_{2.5}$ (phase B, 240 min) sample, and the oxidized $SrCoO_3$ sample (**Figure 3**). Compared to the BM-$SrCoO_{2.5}$ sample, the $H_{1.5}SrCoO_{2.5}$ (phase B) sample is more transparent in the visible region, whereas the oxidized $SrCoO_3$ sample shows lower transmissivity. The as-grown BM-$SrCoO_{2.5}$ samples are brown, the oxidized $SrCoO_3$ sample is black, and the protonated $H_{1.5}SrCoO_{2.5}$ (phase B) sample is colorless transparent, respectively, as shown in the inset photograph. Note that the low transmission in the IR region is due to the absorption of Nb-doped $SrTiO_3$ film. The overall tendency of the color change in the electrochemical cells is similar to the previously reported tendencies in literature[5, 24].

The magnetic properties of the solid-state electrochemical cell were measured (**Figure 4**). The magnetism of $SrCoO_x$ is closely linked to the concentration of oxygen in the

lattice possibly due to the formation of oxygen holes[25-26]. The clear magnetic transition was observed from the *M* versus *T* curve with 100 Oe of the magnetic field through a SQUID magnetometer (**Fig. 4a**). The as-grown BM-$SrCoO_{2.5}$ sample did not show any magnetic transition due to its antiferromagnetic ground state. On the other hand, a clear transition is observed in the oxidized $SrCoO_3$ sample. The transition temperature (T_c) is estimated to be ~240 K, which is comparable to the reported T_c of the nearly stoichiometric perovskite $SrCoO_3$[5, 7-8]. Further, the protonated $H_{1.5}SrCoO_{2.5}$ (phase B) sample showed a weak ferromagnetic behavior with T_c ~130 K, which is consistent with the reported value[5]. We also measured the field-dependent magnetization measurements at 10 K (**Fig. 4b**). The oxidized $SrCoO_3$ sample showed a clear ferromagnetic signal, where the hysteresis loop is clearly seen. The coercive field is estimated to be 500 Oe, which is ~1/4 of the data from the ionic-liquid case (~2000 Oe[5]). Since the $SrCoO_3$ film releases oxygen even at room temperature in air, the measured saturation magnetization is smaller than the references, while the magnetic transition temperature is 240 K, which is close to the transition temperature of nearly stoichiometric $SrCoO_{3-\delta}$. Note that the coercive field of our film is comparable to that of $SrCoO_3$ single crystal. In contrast, the protonated $H_{1.5}SrCoO_{2.5}$ (phase B) sample has a comparable magnetic moment to ionic-liquid gated $HSrCoO_{2.5}$[5]. These results clearly show that the optical and magnetic

properties can be controlled electrochemically at room temperature in air by using the solid-state electrochemical cells composed of $SrCoO_{2.5}$ and CAN solid electrolyte.

Compared to the use of ionic liquid as the electrolyte, our solid-state electrochemical cell has an advantage in terms of being free from the liquid leakage problem. In addition, these results also suggest that the CAN film can be used as the solid electrolyte for the memory device utilizing electrochemical protonation/oxidation of TMOs.

CONCLUSIONS

In summary, we demonstrated a solid-state electrochemical protonation of $SrCoO_{2.5}$ films at room temperature in air. We prepared solid-state electrochemical cells of $SrCoO_{2.5}$ using mesoporous amorphous $12CaO \cdot 7Al_2O_3$ (CAN) film as the solid electrolyte. The electrochemical protonation was performed by applying constant positive voltage (+10 V) to the electrochemical cells. During the protonation treatment, the crystalline phase discretely changed from $SrCoO_{2.5}$ to $HSrCoO_{2.5}$ (phase A), $H_{1.5}SrCoO_{2.5}$ (phase B), and $H_2SrCoO_{2.5}$ (phase C) through formation of an intermediate phase of $H_{1.25}SrCoO_{2.5}$. The $H_{1.5}SrCoO_{2.5}$ (phase B) sample was colorless-transparent

and showed weak ferromagnetism with T_c ~130 K. The present results suggest that the CAN film can be used as the solid electrolyte for the protonation treatment of TMOs.

ASSOCIATED CONTENT

Supporting Information

Supporting Information is available free of charge via the Internet at https://pubs.acs.org/doi/10.1021/acsaelm.XXXXXXX.

Depth profiles of H, Ti, and Co ions of the multilayer samples measured by SIMS (40 μm × 40 μm).

AUTHOR INFORMATION

Corresponding Authors

Qian Yang − Graduate School of Information Science and Technology, Hokkaido University, N14W9, Kita, Sapporo 060-0814, Japan

ORCiD: orcid.org/0000-0002-1916-7025

Email: yangqian@eis.hokudai.ac.jp

Hiromichi Ohta − Research Institute for Electronic Science, Hokkaido University, N20W10, Kita, Sapporo 001-0020, Japan

ORCiD: orcid.org/0000-0001-7013-0343

Email: hiromichi.ohta@es.hokudai.ac.jp

Author

Joonhyuk Lee − Department of Physics, Pusan National University, Geumjeong-gu, Busan 46241, South Korea

ORCiD: orcid.org/ 0000-0001-6014-3319

Hyoungjeen Jeen − Department of Physics, Pusan National University, Busan 46241, South Korea

ORCiD: orcid.org/0000-0003-2922-377X

Hai Jun Cho − Research Institute for Electronic Science, Hokkaido University, N20W10, Kita, Sapporo 001-0020, Japan

ORCiD: orcid.org/0000-0002-8642-4183

Author Contributions

Q.Y. performed the sample preparation and measurements. J.L. and H.J. measured the in-situ XRD patterns and magnetic properties. Q.Y. and H.O. planned and supervised the project. All authors discussed the results and commented on the manuscript.

Funding Sources

Qian Yang received funding from Grants-in-Aid for JSPS Fellows (21J10042).

Hiromichi Ohta received founding from Grants-in-Aid of the JSPS (19H05791).

Notes

The authors declare no competing financial interest.

ACKNOWLEDGEMENTS

This research was supported by Grants-in-Aid for Innovative Areas (19H05791) from the JSPS. Q.Y. was supported by Grants-in-Aid for JSPS Fellows (21J10042) from the JSPS. H.J.J was supported by PNU-RENovation (2020-2021). A part of this work was supported by Dynamic Alliance for Open Innovation Bridging Human, Environment, and Materials, and by the Network Joint Research Center for Materials and Devices.

REFERENCES

1. Hwang, C. S.; Dieny, B. Advanced memory-Materials for a new era of information technology. *MRS Bull.* **2018,** *43*, 330-333.

2. Leighton, C. Electrolyte-based ionic control of functional oxides. *Nat. Mater.* **2019,**

18, 13-18.

3. Tsujimoto, Y.; Tassel, C.; Hayashi, N.; Watanabe, T.; Kageyama, H.; Yoshimura, K.; Takano, M.; Ceretti, M.; Ritter, C.; Paulus, W. Infinite-layer iron oxide with a square-planar coordination. *Nature* **2007,** *450*, 1062-1065.

4. Li, D. F.; Lee, K.; Wang, B. Y.; Osada, M.; Crossley, S.; Lee, H. R.; Cui, Y.; Hikita, Y.; Hwang, H. Y. Superconductivity in an infinite-layer nickelate. *Nature* **2019,** *572*, 624-627.

5. Lu, N.; Zhang, P.; Zhang, Q.; Qiao, R.; He, Q.; Li, H.-B.; Wang, Y.; Guo, J.; Zhang, D.; Duan, Z. Electric-field control of tri-state phase transformation with a selective dual-ion switch. *Nature* **2017,** *546*, 124-128.

6. Katase, T.; Ohta, H. Oxide-based optical, electrical and magnetic properties switching devices with water-incorporated gate insulator. *Jpn. J. Appl. Phys.* **2019,** *58*, 090501.

7. Jeen, H.; Choi, W. S.; Biegalski, M. D.; Folkman, C. M.; Tung, I. C.; Fong, D. D.; Freeland, J. W.; Shin, D.; Ohta, H.; Chisholm, M. F.; Lee, H. N. Reversible redox reactions in an epitaxially stabilized $SrCoO_x$ oxygen sponge. *Nat. Mater.* **2013,** *12*, 1057-1063.

8. Jeen, H.; Choi, W. S.; Freeland, J. W.; Ohta, H.; Jung, C. U.; Lee, H. N. Topotactic phase transformation of the Brownmillerite $SrCoO_{2.5}$ to the Perovskite $SrCoO_{3-\delta}$. *Adv. Mater.* **2013,** *25*, 3651.

9. Li, H. B.; Lou, F.; Wang, Y. J.; Zhang, Y.; Zhang, Q. H.; Wu, D.; Li, Z. L.; Wang, M.; Huang, T. T.; Lyu, Y. J.; Guo, J. W.; Chen, T. Z.; Wu, Y.; Arenholz, E. K.; Lu, N. P.; Wang, O. R. D.; He, Q.; Gu, L.; Zhu, J.; Nan, C. W.; Zhong, X. Y.; Xiang, H. J.; Yu, P. Electric Field-Controlled Multistep Proton Evolution in $H_xSrCoO_{2.5}$ with Formation of H-H Dimer. *Adv. Sci.* **2019,** *6*, 1901432.

10. Lu, Q. Y.; Huberman, S.; Zhang, H. T.; Song, Q. C.; Wang, J. Y.; Vardar, G.; Hunt, A.; Waluyo, I.; Chen, G.; Yildiz, B. Bi-directional tuning of thermal transport in $SrCoO_x$ with electrochemically induced phase transitions. *Nat. Mater.* **2020,** *19*, 655-664.

11. Gao, L.; Chen, X. K.; Lyu, X. Y.; Ji, G. P.; Chen, Z. F.; Zhu, M. T.; Cao, X.; Li, C. R.; Ji, A. L.; Cao, Z. X.; Lu, N. P. Tracing the ionic evolution during ILG induced phase transformation in strontium cobaltite thin films. *J. Phys. Condens. Matter* **2021,** *33*, 104004.

12. Katase, T.; Suzuki, Y.; Ohta, H. Reversibly switchable electromagnetic device with leakage-free electrolyte. *Adv. Electron. Mater.* **2016,** *2*, 1600044.

13. Katase, T.; Suzuki, Y.; Ohta, H. Highly conducting leakage-free electrolyte for $SrCoO_x$-based non-volatile memory device. *J. Appl. Phys.* **2017,** *122*, 135303.

14. Ohta, H.; Sato, Y.; Kato, T.; Kim, S.; Nomura, K.; Ikuhara, Y.; Hosono, H. Field-induced water electrolysis switches an oxide semiconductor from an insulator to a metal. *Nat. Commun.* **2010,** *1*, 118.

15. Ohta, H.; Mizuno, T.; Zheng, S.; Kato, T.; Ikuhara, Y.; Abe, K.; Kumomi, H.; Nomura, K.; Hosono, H. Unusually Large Enhancement of Thermopower in an Electric Field Induced Two-Dimensional Electron Gas. *Adv. Mater.* **2012,** *24*, 740-744.

16. Ohta, H. Electric-field thermopower modulation in $SrTiO_3$-based field-effect transistors. *J. Mater. Sci.* **2013,** *48*, 2797-2805.

17. Katase, T.; Endo, K.; Tohei, T.; Ikuhara, Y.; Ohta, H. Room-Temperature-Protonation-Driven On-Demand Metal-Insulator Conversion of a Transition Metal Oxide. *Adv. Electron. Mater.* **2015,** *1*, 1500063.

18. Katase, T.; Endo, K.; Ohta, H. Infrared-transmittance tunable metal-insulator conversion device with thin-film-transistor-type structure on a glass substrate. *APL*

Mater. **2017,** *5*, 056105.

19. Katase, T.; Onozato, T.; Hirono, M.; Mizuno, T.; Ohta, H. A transparent electrochromic metal-insulator switching device with three-terminal transistor geometry. *Sci. Rep.* **2016,** *6*, 25819.

20. Ohta, H.; Kim, S.; Mune, Y.; Mizoguchi, T.; Nomura, K.; Ohta, S.; Nomura, T.; Nakanishi, Y.; Ikuhara, Y.; Hirano, M.; Hosono, H.; Koumoto, K. Giant thermoelectric Seebeck coefficient of two-dimensional electron gas in $SrTiO_3$. *Nat. Mater.* **2007,** *6*, 129-134.

21. Yang, Q.; Cho, H. J.; Jeen, H.; Ohta, H. Macroscopic visualization of fast electrochemical reaction of $SrCoO_x$ oxygen sponge. *Adv. Mater. Interfaces* **2019,** *6*, 1901260.

22. Yang, Q.; Lee, J.; Feng, B.; Ikuhara, Y.; Kim, G.; Cho, H. J.; Jeen, H.; Ohta, H. Unusually Large Thermopower Change from +330 to -185 $\mu V\ K^{-1}$ of Brownmillerite $SrCoO_{2.5}$. *ACS Appl. Electron. Mater.* **2020,** *2*, 2250-2256.

23. de la Calle, C.; Aguadero, A.; Alonso, J. A.; Fernandez-Diaz, M. T. Correlation between reconstructive phase transitions and transport properties from $SrCoO_{2.5}$ brownmillerite: A neutron diffraction study. *Solid State Sci.* **2008,** *10*, 1924-1935.

24. Choi, W. S.; Jeen, H.; Lee, J. H.; Seo, S. S. A.; Cooper, V. R.; Rabe, K. M.; Lee, H. N. Reversal of the Lattice Structure in $SrCoO_x$ Epitaxial Thin Films Studied by Real-Time Optical Spectroscopy and First-Principles Calculations. *Phys. Rev. Lett.* **2013,** *111*, 097401.

25. Potze, R.; Sawatzky, G.; Abbate, M. Possibility for an intermediate-spin ground state in the charge-transfer material $SrCoO_3$. *Phys. Rev. B* **1995,** *51*, 11501.

26. Medling, S.; Lee, Y.; Zheng, H.; Mitchell, J.; Freeland, J.; Harmon, B. N.; Bridges,

F. Evolution of magnetic oxygen states in Sr-doped $LaCoO_3$. *Phys. Rev. Lett.* **2012,** *109*, 157204.

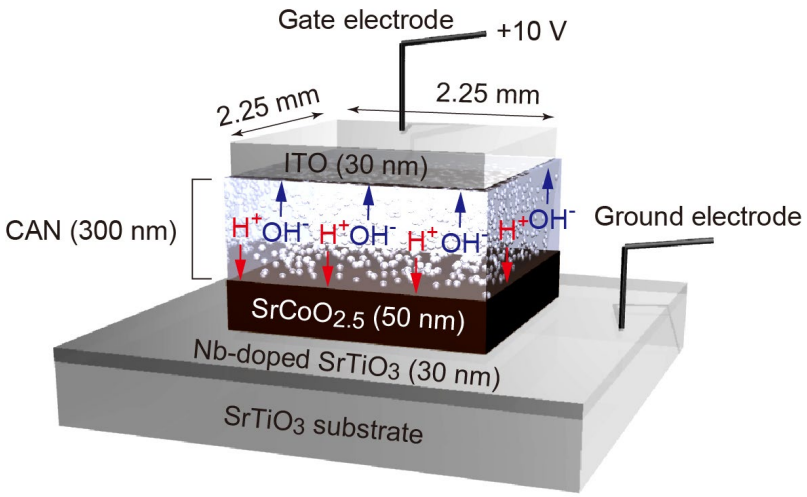

Figure 1. Schematic illustration of solid-state electrochemical protonation of $SrCoO_{2.5}$ film. The active area of the electrochemical cell is 2.25 mm × 2.25 mm. +10 V was applied for the protonation. Since CAN film contains ultrapure water, protonation of $SrCoO_{2.5}$ and oxidation of ITO films occurs during +10 V application.

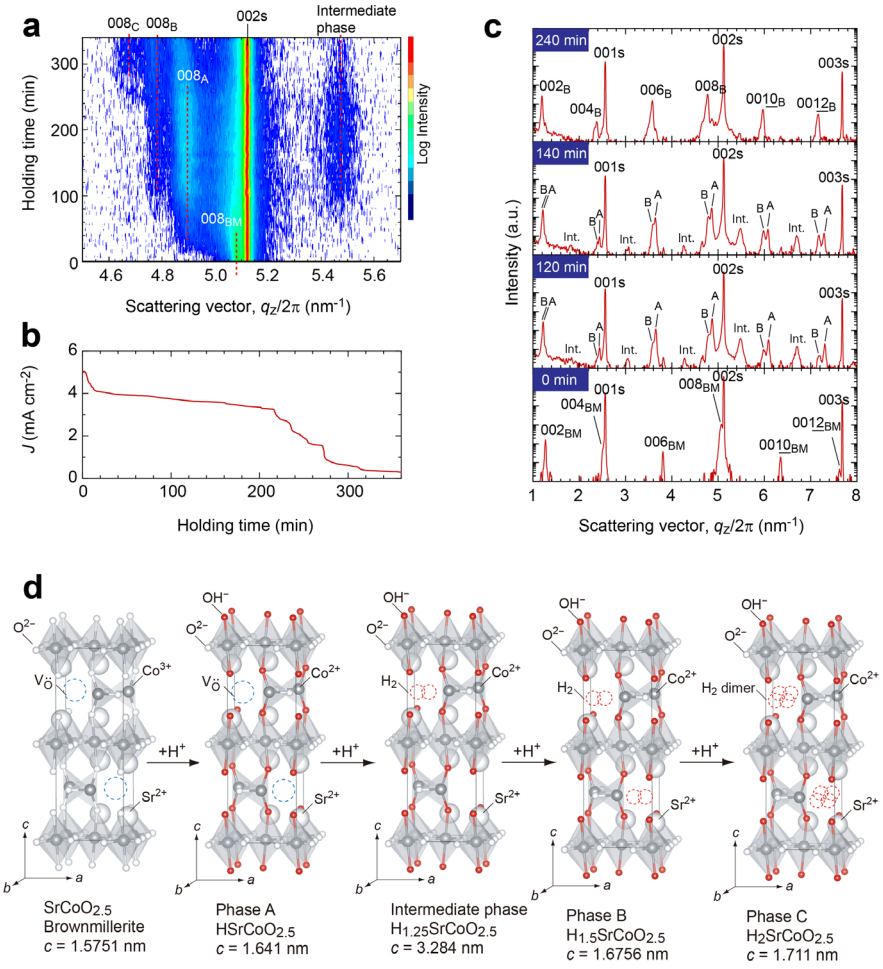

Figure 2. Crystal phase modulation during the protonation. (a) Change in the out-of-plane XRD pattern of the solid-state electrochemical cell during the electrochemical protonation treatment. The XRD patterns were taken every 5 min in situ. (b) Change in the current density (J) with holding time. (c) Out-of-plane XRD patterns of the solid-state electrochemical cell (another sample) after the electrochemical protonation treatment. A, B, and Int. denote $HSrCoO_{2.5}$ (phase A), $H_{1.5}SrCoO_{2.5}$ (phase B), and $H_{1.25}SrCoO_{2.5}$ (intermediate phase), respectively. (d) Schematic crystal structure change upon protonation.

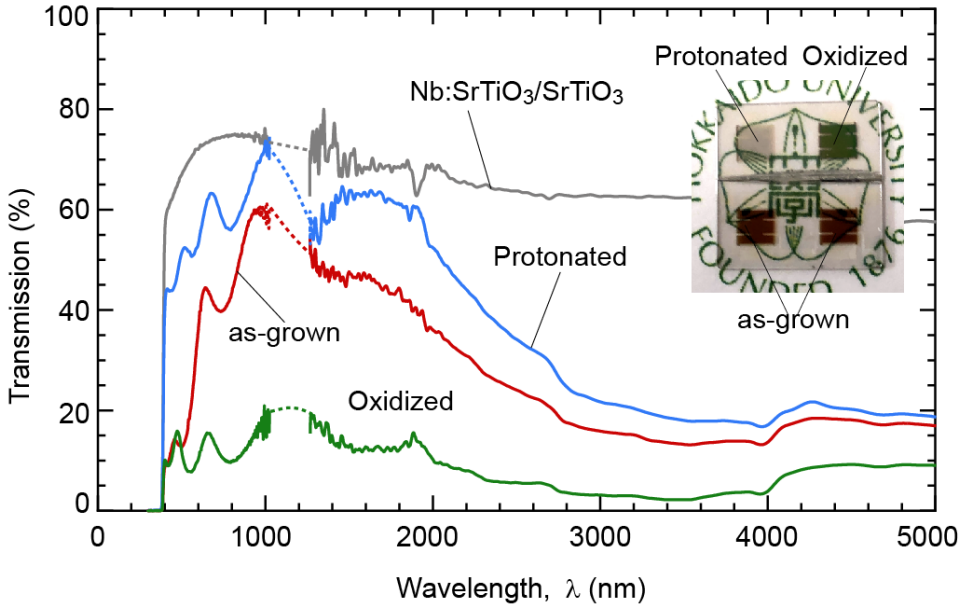

Figure 3. Optical transmission spectra of the solid-state electrochemical cells. As-grown: BM-$SrCoO_{2.5}$ sample, Protonated: $H_{1.5}SrCoO_{2.5}$ sample (240 min, **Fig. 2c**), Oxidized: $SrCoO_3$ sample. The gray line is the reference of Nb:$SrTiO_3$-coated $SrTiO_3$ substrate. The dotted lines were used to connect two different spectrometer results. (Inset) Photograph of the devices. The as-grown BM-$SrCoO_{2.5}$ samples are brown, the protonated $H_{1.5}SrCoO_{2.5}$ sample (240 min) is colorless transparent, and the oxidized $SrCoO_3$ sample is black, respectively. The logomark is reprinted with permission from Hokkaido University.

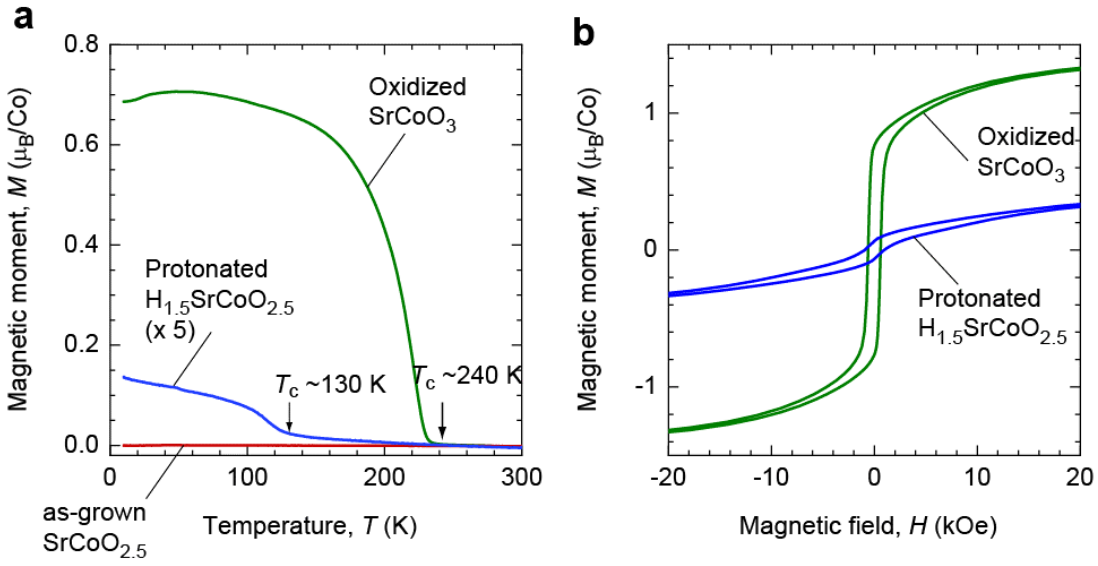

Figure 4. (a) Temperature dependence of the magnetization of $SrCoO_x$ layer measured with the magnetic field of 100 Oe. The oxidized $SrCoO_3$ sample shows clear magnetic transition with T_c ~240 K. The protonated $H_{1.5}SrCoO_{2.5}$ sample (240 min, **Fig. 2c**) shows T_c ~130 K. Both T_c values are comparable to the reported values[5]. (b) M–H curves of the oxidized $SrCoO_3$ sample and the protonated $H_{1.5}SrCoO_{2.5}$ sample measured at 10 K.

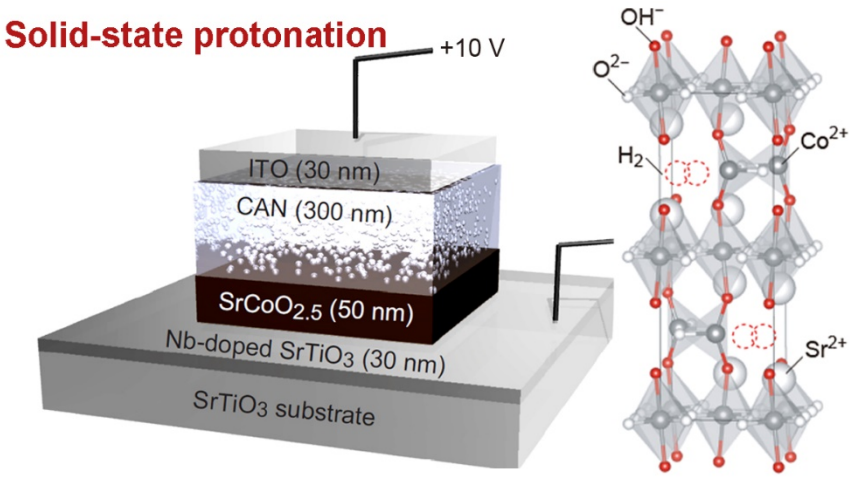
Solid-state protonation
+10 V
ITO (30 nm)
CAN (300 nm)
SrCoO2.5 (50 nm)
Nb-doped SrTiO3 (30 nm)
SrTiO3 substrate
OH−
O2−
H2
Co2+
Sr2+

Supporting Information

Solid-State Electrochemical Protonation of $SrCoO_{2.5}$ into $H_xSrCoO_{2.5}$ (x = 1, 1.5 and 2)

Qian Yang[a*], Joonhyuk Lee[b], Hyoungjeen Jeen[b], Hai Jun Cho[c], and Hiromichi Ohta[c*]

[a] *Graduate School of Information Science and Technology, Hokkaido University, N14W9, Kita, Sapporo 060-0814, Japan*

[b] *Department of Physics, Pusan National University, Busan 46241, South Korea*

[c] *Research Institute for Electronic Science, Hokkaido University, N20W10, Kita, Sapporo 001-0020, Japan*

*Email: yangqian@eis.hokudai.ac.jp, hiromichi.ohta@es.hokudai.ac.jp

KEYWORDS: solid-state electrochemical protonation, brownmillerite, $H_xSrCoO_{2.5}$, $SrCoO_{2.5}$, optical property, magnetic property

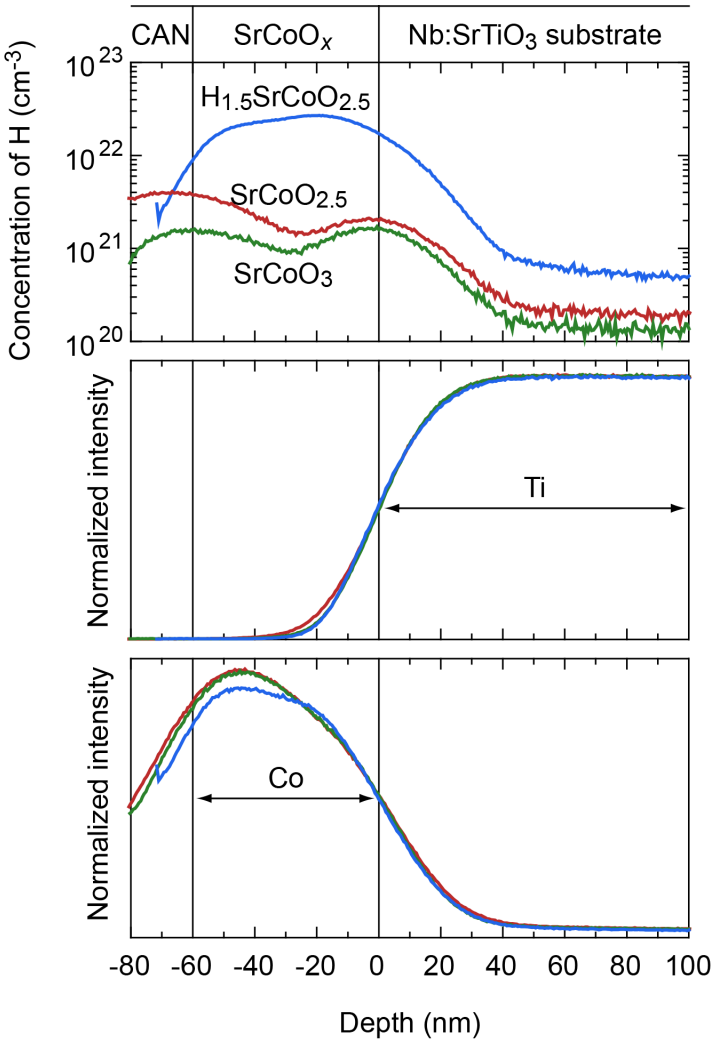

Figure S1. Depth profiles of H, Ti, and Co ions of the multilayer samples measured by SIMS (40 μm × 40 μm). The hydrogen concentration of the protonated $H_{1.5}SrCoO_{2.5}$ sample is ~2 × 10^{22} cm^{-3}, confirmed that $H_{1.5}SrCoO_{2.5}$ was formed. SIMS results do not show a flat profile. This is due to the film surface of ITO/CAN is rough. Since high-density hydrogen is contained in the CAN layer, the H signals of $SrCoO_{2.5}$ and $SrCoO_3$ possibly affected by the CAN layer. Therefore, the large H signal of $SrCoO_{2.5}$ and $SrCoO_3$ would not be a real value.